analytical chemistry

Article

Cite This: Anal. Chem. 2019, 91, 12038−12045

pubs.acs.org/ac

Triple-Helix Molecular Switch Electrochemiluminescence Nanoamplifier Based on a S-Doped Lu_2O_3/Ag_2S Pair for Sensitive MicroRNA Detection

Huan Gao,[†] Junfang Zhang,[†] Ying Liu,[†] Wenwen Tu,[†] Tianxiang Wei,*[,†,‡] and Zhihui Dai*[,†,§]

[†]Jiangsu Collaborative Innovation Center of Biomedical Functional Materials and Jiangsu Key Laboratory of Biofunctional Materials, School of Chemistry and Materials Science and [‡]School of Environment, Nanjing Normal University, Nanjing 210023, People's Republic of China

[§]Nanjing Normal University Center for Analysis and Testing, Nanjing 210023, People's Republic of China

Supporting Information

ABSTRACT: Development of sensitive detection methods for microRNAs has realistic application value for early clinical analysis and accurate diagnosis. In this study, a triple-helix molecular switch electrochemiluminescence resonance energy transfer (ECL-RET) nanoamplifier was designed to construct an electrochemiluminescence (ECL) biosensor for microRNA determination. The newly synthesized S-doped Lu_2O_3, which shows a 3 times better ECL performance than Lu_2O_3, was chosen as the donor in this ECL-RET system. Accordingly, Ag_2S quantum dots (QDs) were used as the matched acceptor. They exhibited overlapping spectra and efficient energy transfer between each other. Furthermore, using a triple-helix switch structure with an improved quenching effect for signal amplification and a nano-DNA walker transformational system as a powerful method for target amplification, a supernanoamplifier was achieved. As a consequence, the proposed ECL biosensor for microRNA-141 detection exhibited good analytical performance with a low detection limit (16 aM). The sensor not only led to the development of a novel ECL-RET pair but also provided a strong nanoamplifier for biosensing platform construction, which may offer some new considerations regarding material design, signal amplification, and show promising application value in biomedical and clinical diagnosis.

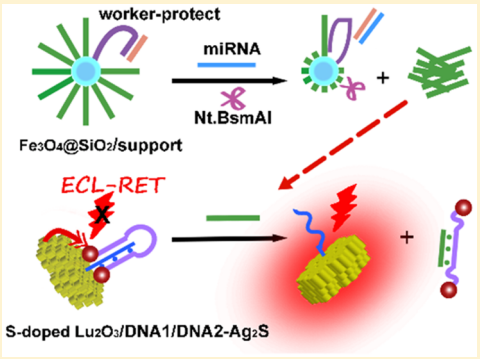

MicroRNAs (miRNAs) are a series of endogenetic, noncoding single-stranded RNAs (ca. 18−24 nt), which are vital regulators in many processes of biological activity, including gene transcription, expression, cellular proliferation, and so on.[1,2] Their aberrant expression is closely associated with some diseases, such as strokes,[3] Parkinson's disease,[4] and different types of cancers.[5,6] Recently, miRNAs have become a class of major and promising biomarker candidates for the early clinical diagnosis of cancer. Nevertheless, due to the intrinsic characteristic of miRNAs, which are of quite low abundance in cells and plasma, the expression level of miRNAs is difficult to quantify. As a consequence, sensitive detection of miRNAs is still a major challenge.[7] Diverse molecular biology-based detection techniques have been used for improving the detection sensitivity, such as polymerase chain reaction (PCR),[8] Northern blotting,[9] and rolling circle amplification.[10] These methods always need high criteria for instruments and reaction conditions. Over the past few decades, many detection techniques like plasmonic, photonic optical, and electrical/electrochemical technologies have been rapidly developed to improve sensitivity and confirmed to be valuable in miRNAs quantitation.[11] Among these approaches, including fluorescence, surface-enhanced Raman spectroscopy, and electrochemical assays, electrochemiluminescence (ECL)-based analysis has been widely explored.[12,13] As the ECL method has the characteristics of low background, easy controllability, and high sensitivity, it offers broad application prospects for determination of multiple biomarkers.

Coupled with resonance energy transfer (RET), analysis performance of ECL can be further enhanced. The ECL-RET system has been used as a successful method for the construction of many biosensors with versatility, low background, and good temporal−spatial control.[14−16] Generally, the ECL-RET system established based on molecular spectroscopy involves efficient energy transfer processes between the donor and an acceptor. The optical spectroscopy response is mainly manifested as spectral to overlap between the donor's emission spectrum and the acceptor's absorption spectrum.[17,18] To implement a sensitive ECL-RET system, two points are needed: a newly synthesized emitter with enhanced ECL signal and an acceptor with reduced noise. Their pairing

Received: July 8, 2019
Accepted: August 16, 2019
Published: August 16, 2019

DOI: 10.1021/acs.analchem.9b03071
Anal. Chem. 2019, 91, 12038−12045

Scheme 1. Schematic Illustration of the As-Proposed Biosensing Platform Based on a Dual Amplification Strategy for microRNA Detection[a]

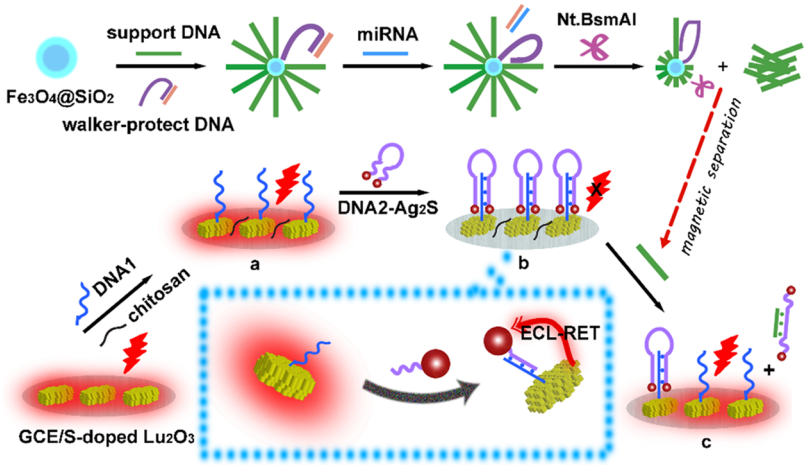

[a](a) Fabrication of aptasensor based on S-doped Lu_2O_3/ DNA1. (b) DNA configuration change for ECL-RET strategy. (c) microRNA detection and ECL signal out.

can greatly improve the sensitivity and lower the signal-to-noise ratio of the ECL-RET system.

In the ECL-RET sensing field, pursuing an innovative luminophore, which has deeply revolutionized and promoted the advancement of ECL biosensors, is never a wasted effort.[19] When choosing the ECL emitter, rare earth materials attract our attention because of their unique 4f electronic configurations along with outstanding optical properties and electro-optic conversion performance. Moreover, their low toxicity could make them suitable biocompatible materials.[20] Lu_2O_3 is a kind of rare earth oxide and photonic material with inherent persistent luminescence emission.[21] Also, lutetia host lattices have become used in several applications, such as medical diagnostic imaging, light-emitting devices, and biosensor construction.[22−24] In this regard, it is expected that Lu_2O_3 would have good performance in ECL applications. Recently, many research studies have shown that doping atoms or ions of appropriate elements into a matrix lattice often enhances the ECL intensity of host material. In Chai's work, ceria-doped ZnO generated a stronger ECL signal than pure ZnO.[25] In addition, Wang's group used ZnO/graphene to fabricate an ECL biosensor. Once the graphene is replaced by nitrogen-doped graphene, the ECL intensity is enhanced approximately 4.3-fold.[26] This phenomenon was mainly caused by the mismatch of size and valence between the doped ions and the matrix material ions, which can further influence the surface state of metal materials and change the ECL signal. In this work, we further modified Lu_2O_3 with nontoxic and environmentally friendly elements through a solvothermal method to obtain S-doped Lu_2O_3 with morphological features of ordered porous and layered structures, which endow them with large surface areas and a promising ability to carry biomolecules.[27] The results show that compared to Lu_2O_3, the newly synthesized S-doped Lu_2O_3 has enhanced ECL performance.

In addition, we developed Ag_2S quantum dots (QDs) as the acceptor for pairing with S-doped Lu_2O_3. The ultraviolet−visible (UV−vis) absorption spectrum of Ag_2S QDs shows a good match with the ECL spectrum of S-doped Lu_2O_3, which means energy transfer can happen between them. To further reduce noise, instead of a traditional hairpin or other double-strand-forming units, a triple-helix switch was applied to build this ECL-RET system.[28,29] This distinctive triplex structure oligonucleotide chain with two armed oligos can label two acceptors, which achieves the same stability and affinity as double-helix DNA in some conditions.[30,31] When triplex-helix DNA (DNA2) is connected with two Ag_2S QDs through amide bonds, the ECL emission shows a relatively higher quenching effect than that of traditional hairpin DNA-linked one Ag_2S QD. Therefore, the DNA molecular conformational change increases the binding number of acceptors and further lowers the noise of this biosensor. With the addition of transformational DNAs, DNA2-Ag_2S are hybridized and leave from the surface of the electrode. This process shows an on−off−on pattern and induces the ECL signal amplification of the first stage.

In addition to signal amplification of broadening response range, target amplification can also increase the sensitivity of detection. In recent years, DNA walker as an emerging amplification method has attracted much interest because of their self-assembly capacity, high payload efficiency, ability to mimic biological phenomena, and strong target amplification capability.[32,33] On this basis, we construct a DNA walker through magnetically responsive silica-coated ferriferrous oxide nanoparticles (Fe_3O_4@SiO_2 NPs) as a platform to effectively load and separate DNAs and combine it with Nt.BsmAI nicking endonuclease to hydrolyze the corresponding recognition sequences. This walker machine can convert trace target miRNAs to numerous transformational DNAs and achieve target amplification of the second stage.

Thus, upon integrating the DNA walker-Fe_3O_4@SiO_2 NPs with the triple-helix molecular switch ECL-RET nanoamplifier of S-doped Lu_2O_3−Ag_2S in our proposed biosensor, we chose miRNA-141 as the model analyte, and an ultrasensitive detection platform was constructed (Scheme 1). With the DNA molecular switch changed, the ECL intensity shows on−off-on behavior. In the initial state, S-doped Lu_2O_3 donor emits a strong ECL intensity (on state, Scheme 1a). After DNA2-Ag_2S complement with DNA1, Ag_2S QDs were attached to the surface of the electrode and got closer to the emitters, which resulted in the decreased ECL response (off state, Scheme 1b). Later, when transformational DNAs were present in the

DOI: 10.1021/acs.analchem.9b03071
Anal. Chem. 2019, 91, 12038−12045

detection system, they specifically hybridize with DNA2-Ag_2S and open triplex-forming switches to obtain double-stranded DNAs (ds-DNAs). The ds-DNAs carry many quenchers that will be released into the aqueous solution (on state, Scheme 1c). After testing with an ECL detector, quantitative evaluation of miRNA-141 can be easily achieved. On the basis of this nanoamplifier, the ECL biosensing platform exhibits a good performance, which is expected not only to provide some new thoughts for the ECL-RET system construction and signal amplification but also to serve as a powerful tool for biomedical and clinical diagnosis.

EXPERIMENTAL SECTION

Materials and Reagents. Lutetium oxide (Lu_2O_3, 99.9%) and oleic acid (OA) were obtained from Aladdin (Shanghai, China). Thiourea (H_2NCSNH_2, >99%), $FeSO_4·7H_2O$, $Fe(NO_3)_3·9H_2O$, $AgNO_3$, NaOH, HCl, $NH_3·H_2O$, *n*-heptane, ethanol, acetic acid, Na_2HPO_4, KH_2PO_4, $K_2S_2O_8$, NaCl, KCl, $K_4Fe(CN)_6$, and $K_3Fe(CN)_6$ were provided by Sinopharm Chemical Reagent Co., Ltd. (China). Ethylene glycol, 1-octadecene (ODE, 90%), monoethanolamine (MEA), chitosan, *N*-hydroxysuccinimide (NHS, 98%), tetraethyl orthosilicate (TEOS, ≥99%), *N*-(3-(dimethylamino)propyl)-*N*′-ethylcarbodiimide (EDC), and 3-aminopropyltriethoxysilane (APTES, ≥98%) were obtained from Sigma-Aldrich Inc. (USA). Glutaraldehyde (GA, 25%, v/v) and 3-mercaptopropionic acid (MPA) were purchased from Alfa Aesar China Ltd. Phosphate-buffered saline (PBS, 20 mM, 0.1 M NaCl, pH = 7.4) was employed as the washing solution to dissolve all sequences except DNA2. The dissolution of DNA2 was carried out in 20 mM PBS (0.1 M NaCl, 2.5 mM $MgCl_2$, pH = 6.0). The testing electrolyte solution was 0.1 M PBS (0.1 M KCl, pH = 7.4) containing 50 mM $K_2S_2O_8$. All high-performance liquid chromatography (HPLC)-purified sequences (Table S1) in our experiments were purchased from Sangon Biotech Co., Ltd. (Shanghai, China). Nt.BsmAI nicking endonuclease (Nt.BsmAI) and Cut Smart buffer were provided by New England Biotechnology Co., Ltd. (Beijing, China).

Apparatus. The ECL measurements were performed at room temperature with ECL instrumentation and a standard three-electrode system. A modified glassy carbon electrode (GCE, 4 mm in diameter) was used as the working electrode; an Ag/AgCl (3 M KCl) and a platinum rod were used as the reference electrode and auxiliary electrode, respectively. The related ECL data were detected with a MPI-A detection system (Remex Electronic Instrument High-Tech, Xi'an, China). Electrochemical impedance spectroscopy (EIS) was carried out in 100 mM KCl ($K_3Fe(CN)_6$:$K_4Fe(CN)_6$, 1:1, 5 mM) with an Autolab PGSTAT302N potentiostat/galvanostat (Metrohm, Netherlands) from 0.1 Hz to 100 kHz at a signal amplitude of 10 mV. Powder X-ray diffraction (PXRD) patterns were obtained using a D/max 2500VL/PC diffractometer (Japan) with graphite-monochromatized Cu Kα radiation (λ = 1.54060 Å) in a 2θ range from 5°to 90°. The scanning electron microscopy (SEM) image was acquired by a JSM-7600F scanning electron microscope (JEOL, Japan). High-resolution transmission electron microscopes (HRTEM, JEM-2010 and JEOL-2100F, Japan) were used to acquire images. The latter was also used to perform elemental mapping and scanning transmission electron microscopy (STEM) with an accelerating voltage of 200 kV. The photoluminescence (PL) spectrum of S-doped Lu_2O_3 was recorded on a Fluoromax-4 spectrofluorometer (Horiba, USA) at an excitation wavelength of 300 nm. The PL spectra of DNA2-Ag_2S, DNA-Alexa Fluor 488, and DNA2-Ag_2S hybridized DNA-Alexa Fluor 488 were acquired by a FLS 1000 instrument (Edinburgh Instruments Ltd., UK) at an excitation wavelength of 488 nm. UV−vis absorption spectra were obtained with a Cary 60 spectrophotometer (Agilent, USA). Fourier transform infrared (FTIR) spectra were obtained on a Tensor 27 instrument (Bruker, Germany).

Synthesis of Magnetically Responsive Fe_3O_4 NPs. Water-soluble magnetically responsive Fe_3O_4 NPs were synthesized based on a previous report.[34] First, 1.5 M NaOH solution, 0.5 M $FeSO_4$ solution with 0.2 M HCl, and 1 M $Fe(NO_3)_3$ solution with 0.2 M HCl were separately prepared. Then 100 mL of the NaOH solution was added to a three-necked flask (250 mL) and heated to 80 °C. Next, 10 mL of $FeSO_4$ solution and 10 mL of $Fe(NO_3)_3$ solution were added dropwise to the flask under N_2 atmosphere and kept at 80 °C. After 30 min the system was naturally cooled with continuous stirring. The black Fe_3O_4 NPs were collected and washed four times with a water−ethanol mixture (v/v, 1/1).

Synthesis of Magnetically Responsive Silica-Coated Fe_3O_4 NPs. The magnetically responsive Fe_3O_4@SiO_2 NPs were synthesized based on a previous report with some modifications.[35] The prepared Fe_3O_4 NPs were well dispersed in H_2O (100 mL) and stored at 4 °C in the dark for further use. First, 4 mL of Fe_3O_4 solution and 56 mL of ethanol were added into a 100 mL flask under continuous stirring at room temperature. Then 500 μL of $NH_3·H_2O$, 1 mL of TEOS, and 250 μL of APTES were slowly added to the flask at room temperature. After 18 h, the dark brown Fe_3O_4@SiO_2 NPs were washed with ethanol and water and then dried in a vacuum oven.

Synthesis of Carboxylic Acid-Terminated Ag_2S QDs. Ag_2S-COOH QDs were synthesized based on previous reports.[36,37] First, 0.3 mmol of $AgNO_3$ (51 mg), 7 mmol of MPA (610 μL), and ethylene glycol (4.5 mL) were mixed with continuous magnetic stirring until the mixture turned into a homogeneous cloudy white suspension. Then the reactor was degassed for over 10 min and refilled with high-purity argon. The reaction system was heated to 145 °C for 25 min. The color of the mixture changed to transparent yellow and gradually became deep dark. The prepared Ag_2S QDs were washed using water. Finally, the recollected product was stored at 4 °C for further use.

Synthesis of S-Doped Lu_2O_3. S-Doped Lu_2O_3 was prepared using a solvent thermal synthesis method in which a source of S is reduced and introduced into the reaction mixture. First, 1 mmol of Lu_2O_3 (0.398 g) and 6 mmol of H_2NCSNH_2 (0.4567 g) were mixed with OA (3 mL) and ODE (5 mL) under continuous stirring at 60 °C in a water bath. After stirring for 60 min, the solution was transferred into a 50 mL Teflon container. The reaction vessel was heated in an oven at 180 °C and kept for 36 h. Finally, the product was collected and washed four times using *n*-heptane and ethanol (1:1, v/v) and then dried at room temperature in a vacuum oven overnight. Before preparation of the sample aqueous, ultrasonic dissolution is needed.

Preparation of Transformational DNAs. First, 5 μM walker probe solution (20 μL) and 2.5 μM protecting probe solution (20 μL) were mixed, heated at 95 °C for 5 min, and then naturally cooled to obtain ds-DNAs. Whereafter, ds-DNAs (10 μL), 25 μM support DNA (10 μL), and 15 mg·mL^{-1} Fe_3O_4@SiO_2 NPs (20 μL) were blended in PBS (40 μL,

DOI: 10.1021/acs.analchem.9b03071
Anal. Chem. 2019, 91, 12038−12045

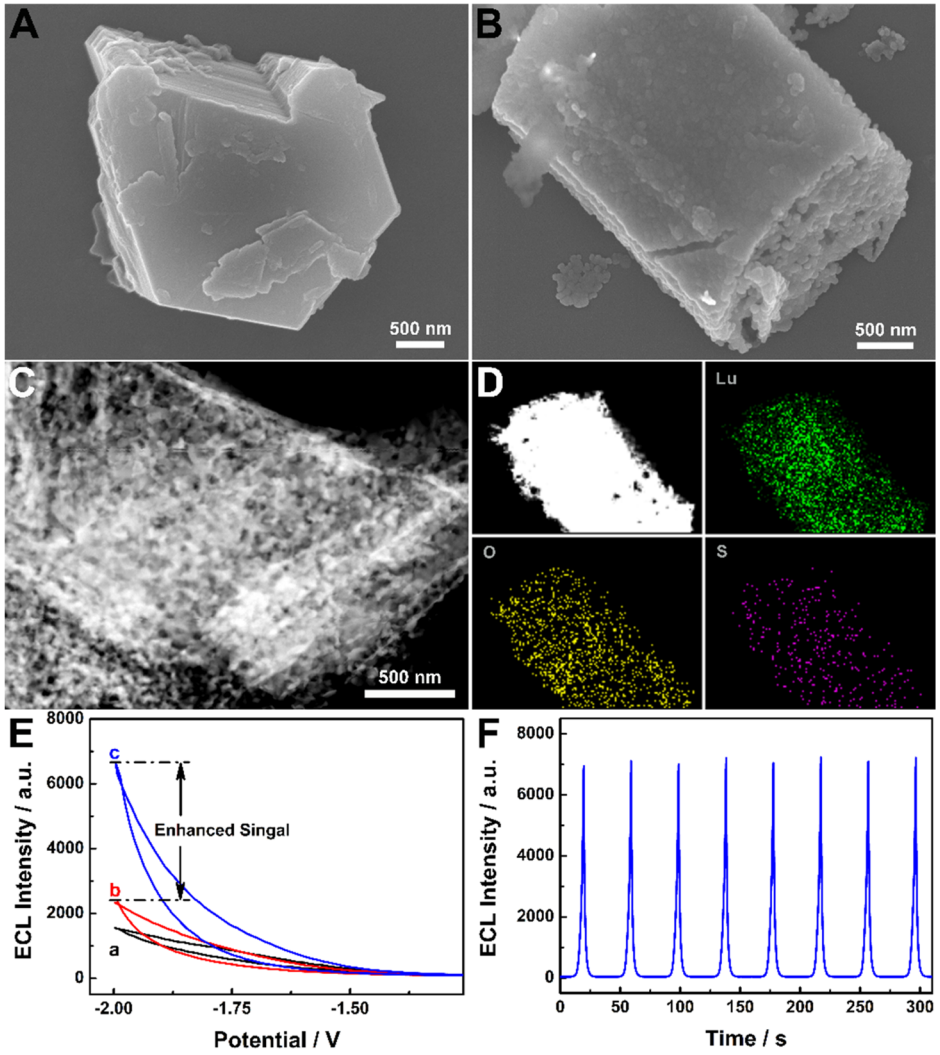

Figure 1. SEM image of bulk layered Lu_2O_3 (A) and S-doped Lu_2O_3 (B). STEM image (C) and mapping images (D) of S-doped Lu_2O_3. (E) ECL potential curves of the GCE (a), Lu_2O_3 (b), and S-doped Lu_2O_3 (c) modified GCEs in 0.1 M PBS buffer (0.1 M KCl, pH = 7.4) containing 50 mM $K_2S_2O_8$. (F) ECL stability test of S-doped Lu_2O_3-modified GCE under eight cyclic potential scans (n = 3).

pH = 7.4). DNA sequences were linked to the surface of Fe_3O_4@SiO_2 NPs by the classic EDC coupling reaction with 20 mg·mL^{-1} EDC (10 μL) and 10 mg·mL^{-1} NHS (10 μL) for 60 min at 37 °C. Afterward, the mixture was sufficiently magnetically separated to obtain DNAs-Fe_3O_4@SiO_2. When different concentrations of miRNA-141 (50 μL) were added, walker probes will be released and further hybridized with support probes for 60 min at 37 °C. Subsequently, 10 U Nt.BsmAI and Cutsmart buffer were added and kept 120 min at 37 °C to cut the recognition sites and produced transformational DNAs. Finally, numerous transformational DNAs were acquired after magnetic separation.[38,39]

Preparation of DNA2-Ag_2S. The prepared Ag_2S QDs were dispersed in 1.0 L of 20 mM PBS (pH = 6.0) and stored at 4 °C. Next, 10 μM DNA2 (10 μL) and an aqueous solution of Ag_2S QDs (50 μL) were mixed. DNA2 were linked to Ag_2S QDs through the EDC coupling reaction with 20 mg·mL^{-1} of EDC (2.5 μL) and 10 mg·mL^{-1} of NHS (2.5 μL) for 60 min at 37 °C. The process of linking hairpin DNAs to Ag_2S QDs was similar to that of preparing DNA2-Ag_2S.

Fabrication of the ECL Biosensor. The GCE was polished by Al_2O_3 powders and washed several times with water. Then it was dried using nitrogen before 2 mg·mL^{-1} S-doped Lu_2O_3 solution (10 μL) was dropped onto the surface. After drying at room temperature for 5 h, 4 μL of chitosan–acetic acid solution (0.1%, wt) was added to the electrode surface and kept overnight. After that the electrode was immersed in 600 μL of 0.25% (v/v) GA solution for 1 h at 25 °C. Rinsing carefully with 60 μL of washing solution, 100 nM DNA1 (10 μL) was cast onto the electrode surface for 60 min and kept at 37 °C. Subsequently, the modified electrode was washed mildly and immersed in 500 μM of MEA solution at 37 °C for 60 min to reduce the number of nonspecific adsorption sites. Afterward, the further modified electrode was incubated with DNA2-Ag_2S (10 μL) for 90 min at 25 °C. The detailed procedure of decorating the electrode with hairpin-linked Ag_2S QDs was the same as that for DNA2-Ag_2S. Finally, after rinsing thoroughly, ECL measurements were recorded between −2.0 and 0 V (scan rate 100 mV s^{-1}) at the voltage of the photomultiplier tube (800 V).

RESULTS AND DISCUSSION

Materials Characterization. Lu_2O_3 is a kind of rare earth oxide which has good dispersibility for wide application in a water system. The bulk-layered Lu_2O_3 shows the structural

DOI: 10.1021/acs.analchem.9b03071
Anal. Chem. 2019, 91, 12038−12045

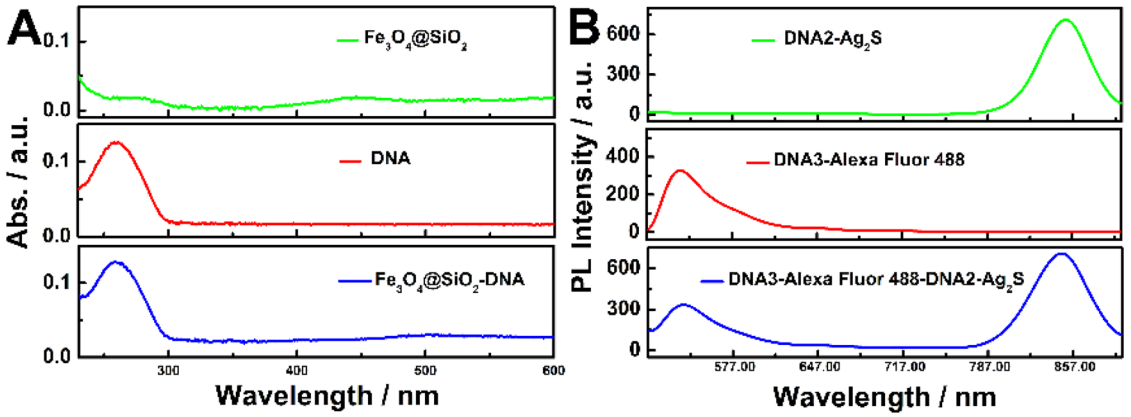

Figure 2. (A) UV−vis absorption spectra of Fe_3O_4@SiO_2 NPs, DNA sequences, and Fe_3O_4@SiO_2 NPs linked with DNA sequences. (B) PL spectra of DNA2-Ag_2S, DNA3-Alexa Fluor 488, and DNA2-Ag_2S hybridized DNA3-Alexa Fluor 488.

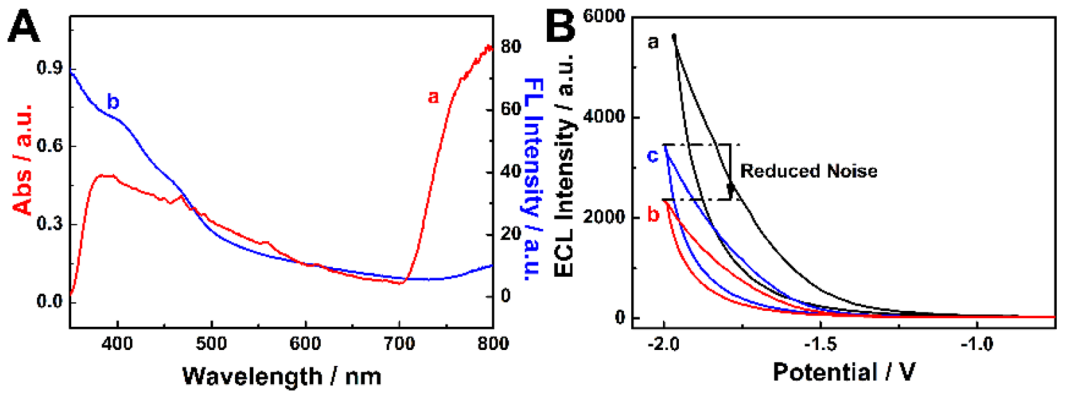

Figure 3. (A) PL spectrum of S-doped Lu_2O_3 (a), and UV−vis absorption spectrum of Ag_2S QDs (b). (B) Comparison of the ECL intensity quenching effect of DNA2-Ag_2S (b) and hairpin DNAs linked with Ag_2S QDs (c) on DNA1/S-doped Lu_2O_3/GCE (a).

feature of several sheets overlapping each other (Figure 1A). On the basis of this character, S-doped Lu_2O_3 was synthesized by a one-step solvothermal etching method. SEM and STEM techniques were employed to distinguish the morphology of S-doped Lu_2O_3. As depicted in Figure 1B and 1C, S-doped Lu_2O_3 has hierarchical porosity, which can help to carry more biomolecules.[27] TEM images further demonstrate the structure character of the porous media clearly (Figure S1AB). It also shows good solubility (Figure S2). Compared to the PXRD pattern of S-doped Lu_2O_3 and Lu_2O_3, both of them display diffraction peaks corresponding to Lu_2O_3 (JCPDS 43-1021) (Figure S3), which demonstrates that the crystal structure remains unchanged. As shown in elemental mapping, different colored dots correspond to distributed Lu, O, and S elements, suggesting that these three elements are scattered evenly (Figure 1D).

After that the ECL performance of newly synthesized S-doped Lu_2O_3 was tested. As shown in Figure 1E, the initial potential of S-doped Lu_2O_3 is −1.35 V. Compared to Lu_2O_3, S-doped Lu_2O_3 achieved an approximately 3-fold increase in ECL intensity. Figure 1F presents the relatively stable ECL signal of S-doped Lu_2O_3 over eight cycles, demonstrating that it has persistent emission. Furthermore, the relative standard deviation is 2.1%. The increased ECL performance of Lu_2O_3 can be attributed to chemical doping, which can effectively modulate the electronic density and improve the charge-transfer rate.[40] In addition, the hierarchical porosity morphology of S-doped Lu_2O_3 provides more active sites, which improves the ECL property and surface chemical reactivity.

The morphologies of Ag_2S QDs, Fe_3O_4 NPs, and Fe_3O_4@SiO_2 NPs were characterized using HRTEM. Ag_2S QDs were monodisperse NPs, approximately 6 nm in width (Figure S4). The hydrophilic Fe_3O_4 NPs (Figure S5A) and Fe_3O_4@SiO_2 NPs (Figure S5B) were spherical with diameters of ∼10 and ∼20 nm, respectively. Crystallization of Fe_3O_4 NPs and Fe_3O_4@SiO_2 NPs was confirmed by the PXRD patterns (Figure S6), in which the main diffraction peaks corresponded to Fe_3O_4 (JCPDS 01-1111). In addition, the broad peak of Fe_3O_4@SiO_2 NPs from 22° to 28° indicated that silica was successfully coated onto the surface of Fe_3O_4 NPs.[35] DNA2-Ag_2S were formed through amide bonds between the carboxyl groups of Ag_2S QDs and the amino groups of DNA2. As shown in the FTIR spectrum, the characteristic peaks of C═O stretching and C−O stretching appeared, suggesting that carboxylic acids of Ag_2S QDs were successfully capped by MPA (Figure S7). The amine-terminated Fe_3O_4@SiO_2 NPs were also investigated by FTIR spectroscopy, which confirmed the presence of amino groups and silica shells (Figure S8). The sample exhibited a broad band, corresponding to Si−O−Si stretching vibrations and N−H bending vibrations. The magnetism of Fe_3O_4 before (Figure S9A) and after (Figure S9B) being coated with silica was confirmed by a hand magnet.

Characterization of the ECL Biosensor. To confirm that DNA sequences were successfully connected with Fe_3O_4@SiO_2 NPs, their UV−vis absorption spectra were investigated

DOI: 10.1021/acs.analchem.9b03071
Anal. Chem. 2019, 91, 12038−12045

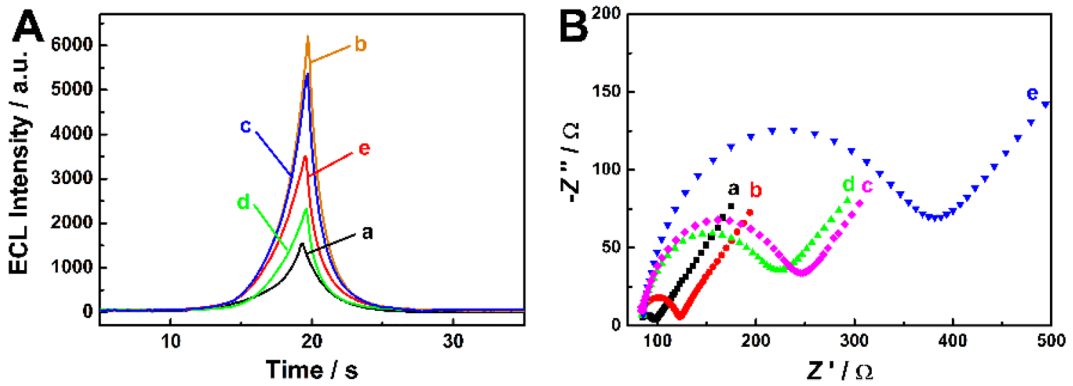

Figure 4. (A) ECL responses of this biosensor during the layer-by-layer construction process: GCE (a), S-doped Lu_2O_3/GCE (b), DNA1/S-doped Lu_2O_3/GCE (c), DNA2-Ag_2S/DNA1/S-doped Lu_2O_3/GCE (d), and DNA2-Ag_2S/DNA1/S-doped Lu_2O_3/GCE incubated with transformational DNAs (e, miRNA-141 = 50 fM). (B) Nyquist plots of (a) bare GCE and different modified electrodes: (b) S-doped Lu_2O_3/GCE, (c) DNA1/S-doped Lu_2O_3/GCE, (d) DNA2-Ag_2S/DNA1/S-doped Lu_2O_3/GCE, and (e) transformational DNAs/DNA2-Ag_2S/DNA1/S-doped Lu_2O_3/GCE.

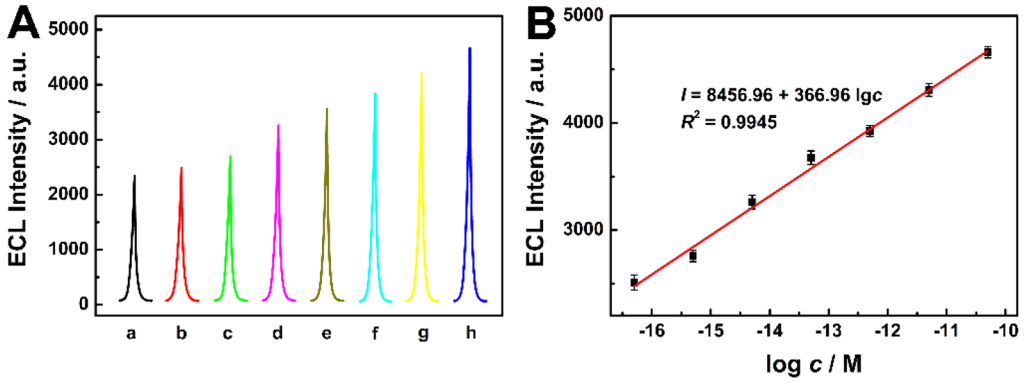

Figure 5. (A) ECL intensity−time curves of the proposed biosensor for detection of miRNA-141 (a, b, c, d, e, f, g, and h: 0 fM, 0.05 fM, 0.5 fM, 5 fM, 50 fM, 0.5 pM, 5 pM, and 50 pM) in 0.1 M PBS (0.1 M KCl, pH = 7.4) containing 50 mM $K_2S_2O_8$. (B) Corresponding calibration plot between the logarithm of the miRNA-141 concentration and the ECL response.

(Figure 2A). Fe_3O_4@SiO_2 NPs and DNA sequences show absorption bands at 450 and 260 nm, respectively. Put DNA sequences into the aqueous solution of Fe_3O_4@SiO_2 NPs and reacted at 37 °C for 60 min, absorption spectrum of the mixture showed a characteristic absorption band of DNA sequences at 260 nm, indicating the successful modification of Fe_3O_4@SiO_2 NPs with DNA sequences. Similarly, PL spectra were utilized to prove the conjugation between Ag_2S QDs and DNA2 (Figure 2B). We designed a DNA3 sequence that was partially complementary to DNA2 and hybridized DNA3-Alexa Fluor 488 with DNA2-Ag_2S. After hybridization, the conjugate was obtained by centrifugation. The PL spectrum was used to verify the effective binding between DNA2 and Ag_2S. DNA2-Ag_2S and DNA3-Alexa Fluor 488 show emission bands at 850 and 535 nm at a 488 nm excitation wavelength, respectively. Under the above experimental conditions, the mixture showed a distinct band, which means the combination between Ag_2S QDs and DNA2 was achieved. To effectively investigate the feasibility of this ECL biosensor on the basis of signal amplification by ECL-RET effect, emission spectrum of S-doped Lu_2O_3 and absorption spectrum of Ag_2S QDs were monitored (Figure 3A). Apparently, a large spectral overlap between the emission of S-doped Lu_2O_3 and the absorption of Ag_2S QDs was observed, which would be beneficial to inducement of the ECL-RET effect. Moreover, we compared the quenching effect of DNA2-Ag_2S (Figure 3B, curve b) with that of the traditional hairpin DNAs-linked Ag_2S QDs (curve c). Ag_2S-DNA2 dramatically reduced the ECL intensity of the proposed biosensor (curve a) and showed lower background noise. Due to the special weak acid reaction environment (pH = 6.0) of DNA2, we need to explore the stability of Ag_2S QDs. Newly synthesized and after 24 h placed in 20 mM PBS (2.5 mM $MgCl_2$, 0.1 M NaCl, pH = 6.0), the absorbance of Ag_2S QDs was little changed (Figure S10).

The ECL responses during stepwise assembly were recorded (Figure 4A). GCE exhibited the lowest ECL response (curve a). An enormous increase in ECL intensity was observed after GCE was modified with S-doped Lu_2O_3 (curve b). When DNA1 was attached onto the electrode surface, the ECL intensity slightly decreased (curve c). After pairing with DNA2-Ag_2S, the ECL intensity further decreased (curve d), which was caused by the ECL-RET effect between Ag_2S QDs and S-doped Lu_2O_3. When transformational DNAs were hybridized with DNA2, the ECL signal recovered (curve e). These phenomena confirm that the proposed ECL biosensor was successfully constructed.

During the stepwise assembly process, EIS of our designed ECL sensor shows changing electron transfer resistance (R_{et}, Figure 4B). GCE shows the lowest R_{et} value (curve a). After S-doped Lu_2O_3 were coated on the surface of GCE, the R_{et} value increased (curve b), because the materials block the electron transfer. When DNA1 were linked onto the electrode, a larger semicircle formed because DNA molecules further hinder the electron transfer (curve c). Following the assembly of DNA2-

DOI: 10.1021/acs.analchem.9b03071
Anal. Chem. 2019, 91, 12038−12045

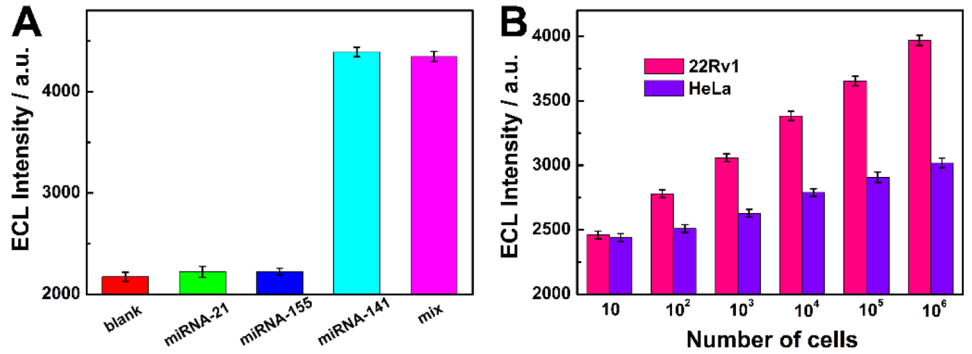

Figure 6. (A) Selectivity analysis of the proposed biosensor toward the blank, miRNA-141 (5 pM), miRNA-21 (50 pM), miRNA-155 (50 pM), and a mixture of miRNA-155 (50 pM), miRNA-21 (50 pM), and miRNA-141 (5 pM). (B) Application of ECL sensing for miRNA-141 analysis in 22Rv1 and HeLa cell lines: 10, 10^2, 10^3, 10^4, 10^5, and 10^6 cells.

Ag_2S, a slightly lower R_{et} could be observed, which indicated successful modification of Ag_2S QDs (curve d). As a semiconductor, Ag_2S QDs could improve the conductivity of the detecting system and facilitate a redox probe shift when placed near the electrode surface. Subsequently, the modified electrode was incubated with transformational DNAs, and hybridization occurred between transformational DNAs and DNA2-Ag_2S, causing the R_{et} value to increase (curve e).

Optimal Conditions for the ECL Biosensor. The effects of the concentration of S-doped Lu_2O_3 and cleaving time of Nt.BsmAI on the ECL signal were investigated to confirm the optimal experimental conditions. As shown in Figure S11A, when the concentration of S-doped Lu_2O_3 increased in the range from 0.1 to 3.0 mg·mL^{-1}, the ECL response increased and reached a maximum at 2.0 mg·mL^{-1}. Hence, 2.0 mg·mL^{-1} was chosen as the optimal concentration of S-doped Lu_2O_3. Figure S11B illustrates the influence of the cleaving time of Nt.BsmAI on this biosensor. When the incubation time was prolonged from 30 to 150 min, the ECL intensity increased and achieved a maximum at 120 min. Therefore, the optimal cleaving time of Nt.BsmAI in this experiment was 120 min.

Analytical Performance of the ECL Biosensor. Under the above optimized conditions, the proposed biosensor was used for quantitative determination of target. As the concentration of miRNA-141 increased, this designed biosensor exhibited a stepwise change in ECL intensity (Figure 5A). A good linear relationship between the ECL signal and the logarithm of miRNA-141 concentration was observed (Figure 5B). The regression equation could be determined as I = 8456.96 + 366.96 lg c with a relatively wide linear range (from 50 aM to 50 pM) and a correlation coefficient of 0.9945 (c is the concentration of miRNA-141, M). The detection limit is 16 aM with 3σ rule (σ is the standard deviation in the blank solution after repeated measurements), which confirms the proposed ECL biosensor has a good analytical performance.[41] Several other existing detection methods of miRNA are listed in Table S2. It can be found that the proposed biosensor shows superior or comparable detection sensitivity to those of the other methods. Furthermore, the selectivity of this ECL biosensor was also investigated by testing miRNA-141 and different sequences (miRNA-21, miRNA-155, and their mixture); the results obtained under the same conditions are displayed in Figure 6A. When other miRNAs were present, signal values were nearly the same as those of the blank sample. However, an increase in ECL intensity happened when miRNA-141 was present, implying the high selectivity of this ECL biosensor for miRNA-141 detection.

Application of the ECL Biosensor in Tumor Cells. For practical assessment of the proposed biosensor in real samples, the expression of miRNA-141 by biological cell lysates from 22Rv1 (human prostate cancer cells) and HeLa (human cervical cancer cells) was further investigated. Figure 6B shows that the ECL responses were enhanced significantly as the number of 22Rvl cells increased from 10 to 10^6, suggesting a high expression level of miRNA-141 in 22Rv1 cells. However, the ECL intensity of the HeLa cell lysate increased slowly, illustrating the low expression level of miRNA-141 in HeLa cells. The experimental results were consistent with a previous report.[42] Given all of the above test results, this sensing platform based on a dual-amplification strategy exhibited a favorable potential in miRNA testing and early diagnostics.

CONCLUSIONS

A novel ECL biosensor with a triple-helix molecular switch ECL-RET nanoamplifier was proposed for microRNA-141 determination. The newly synthesized S-doped Lu_2O_3 and Ag_2S QDs were used as the donor and acceptor, respectively. Through coupling with a triple-helix switch structure an improved quenching effect was achieved. We also used a nano-DNA walker transformational platform for target amplification. Using miRNA-141 as a model analyte,this ECL biosensor shows high sensitivity and a wide linear range. With all of these features, the proposed ECL biosensor with a novel ECL-RET system and a strong nanoamplifier may provide some new considerations for materials design and serve as an applicable tool in biomedical and clinical analysis.

ASSOCIATED CONTENT

Supporting Information

The Supporting Information is available free of charge on the ACS Publications website at DOI: 10.1021/acs.analchem.9b03071.

Oligonucleotide sequences used in this work, TEM images of S-doped Lu_2O_3, photograph of the aqueous of S-doped Lu_2O_3, PXRD patterns of Lu_2O_3 and S-doped Lu_2O_3, HRTEM image of Ag_2S QDs, HRTEM images of Fe_3O_4 NPs and Fe_3O_4@SiO_2 NPs, PXRD assays of Fe_3O_4 NPs and Fe_3O_4@SiO_2 NPs, FTIR spectrum of Ag_2S-COOH QDs, FTIR spectrum of Fe_3O_4@SiO_2-NH_2 NPs, magnetism tests of Fe_3O_4 NPs and Fe_3O_4@SiO_2 NPs, stability test of Ag_2S QDs in weak acid

DOI: 10.1021/acs.analchem.9b03071
Anal. Chem. 2019, 91, 12038−12045

reaction environment, optimal conditions of the ECL biosensor, comparative data of this ECL biosensor and other methods (PDF)

AUTHOR INFORMATION

Corresponding Authors

*Tel./Fax: +86-25-85891051. E-mail: daizhihuii@njnu.edu.cn.
*Tel./Fax: +86-25-85891051. E-mail: weitian_xiang@126.com.

ORCID

Wenwen Tu: 0000-0002-0281-2649
Zhihui Dai: 0000-0001-7049-7217

Author Contributions

The manuscript was written through the contributions of all the authors. All authors have given approval to the final version of the manuscript.

Notes

The authors declare no competing financial interest.

ACKNOWLEDGMENTS

This work was supported by the National Natural Science Foundation of China (21625502 and 21705079) and the Natural Science Foundation of Jiangsu Province (BK20171033). We appreciate the financial support from the Priority Academic Program Development of the Jiangsu Higher Education Institutions and the Program for Jiangsu Collaborative Innovation Center of Biomedical Functional Materials.

REFERENCES

(1) Turchinovich, A.; Weiz, L.; Langheinz, A.; Burwinkel, B. *Nucleic Acids Res.* **2011**, *39* (16), 7223−7233.
(2) Rachagani, S.; Macha, M. A.; Heimann, N.; Seshacharyulu, P.; Haridas, D.; Chugh, S.; Batra, S. K. *Adv. Drug Delivery Rev.* **2015**, *81*, 16−33.
(3) Bam, M.; Yang, X.; Sen, S.; Zumbrun, E. E.; Dennis, L.; Zhang, J.; Nagarkatti, P. S.; Nagarkatti, M. *Mol. Neurobiol.* **2018**, *55* (2), 1419−1429.
(4) Thome, A. D.; Harms, A. S.; Volpicelli-Daley, L. A.; Standaert, D. G. *J. Neurosci.* **2016**, *36* (8), 2383−2390.
(5) Dolai, S.; Sia, K. C.; Robbins, A. K.; Zhong, L.; Heatley, S. L.; Vincent, T. L.; Hochgräfe, F.; Sutton, R.; Kurmasheva, R. T.; Revesz, T.; White, D. L.; Houghton, P. J.; Smith, M. A.; Teachey, D. T.; Daly, R. J.; Raftery, M. J.; Lock, R. B. *Cancer Res.* **2016**, *76* (9), 2766−2777.
(6) Rupaimoole, R.; Calin, G. A.; Lopez-Berestein, G.; Sood, A. K. *Cancer Discovery* **2016**, *6* (3), 235−246.
(7) Cheng, G. *Adv. Drug Delivery Rev.* **2015**, *81*, 75−93.
(8) Liu, C.; Liu, R. F.; Zhang, D. X.; Deng, Q.; Liu, B. G.; Chao, H. P.; Rycaj, K.; Takata, Y.; Lin, K.; Lu, Y.; Zhong, Y.; Krolewski, J.; Shen, J. J.; Tang, D. G. *Nat. Commun.* **2017**, *8*, 14270−14283.
(9) Jou, A. F.; Lu, C. H.; Ou, Y. C.; Wang, S. S.; Hsu, S. L.; Willner, I.; Ho, J. A. *Chem. Sci.* **2015**, *6* (1), 659−665.
(10) Marx, V. *Nat. Methods* **2015**, *12* (5), 393−397.
(11) Graybill, R. M.; Bailey, R. C. *Anal. Chem.* **2016**, *88* (1), 431−450.
(12) Lu, L. P.; Wang, J. X.; Miao, W. J.; Wang, X. Y.; Guo, G. S. *Anal. Chem.* **2019**, *91* (2), 1452−1459.
(13) Liu, Z. Y.; Qi, W. J.; Xu, G. B. *Chem. Soc. Rev.* **2015**, *44* (10), 3117−3142.
(14) Wu, M. S.; Chen, Z. Q.; Xu, H. Y.; Zhang, A. P. *Sci. China: Chem.* **2017**, *60* (3), 410−414.
(15) Yang, X. L.; Tang, Y. N.; Mason, S. D.; Chen, J. B.; Li, F. *ACS Nano* **2016**, *10* (2), 2324−2330.
(16) Zhang, H. Q.; Lai, M.; Zuehlke, A.; Peng, H. Y.; Li, X. F.; Le, X. C. *Angew. Chem., Int. Ed.* **2015**, *54* (48), 14326−14330.
(17) Zhong, X. L.; Chervy, T.; Zhang, L.; Thomas, A.; George, J.; Genet, C.; Hutchison, J. A.; Ebbesen, T. W. *Angew. Chem., Int. Ed.* **2017**, *56* (31), 9034−9038.
(18) Wang, J.; Zhao, W. W.; Zhou, H.; Xu, J. J.; Chen, H. Y. *Biosens. Bioelectron.* **2013**, *41* (15), 615−620.
(19) Wu, M. S.; He, L. J.; Xu, J. J.; Chen, H. Y. *Anal. Chem.* **2014**, *86* (9), 4559−4565.
(20) Bünzli, J. G. *Chem. Rev.* **2010**, *110* (5), 2729−2755.
(21) Zhu, W.; Saddam Khan, M.; Cao, W.; Sun, X.; Ma, H.; Zhang, Y.; Wei, Q. *Biosens. Bioelectron.* **2018**, *99* (15), 346−352.
(22) Chen, Y.; Zhou, S. W.; Li, L. L.; Zhu, J. J. *Nano Today* **2017**, *12*, 98−115.
(23) Kulesza, D.; Bolek, P.; Bos, A. J.J.; Zych, E. *Coord. Chem. Rev.* **2016**, *325* (15), 29−40.
(24) Shen, W. Q.; Zhang, L.; Zheng, S. S.; Xie, Y. P.; Lu, X. *ACS Appl. Mater. Interfaces* **2017**, *9* (34), 28838−28843.
(25) Wang, J. X.; Zhuo, Y.; Zhou, Y.; Wang, H. J.; Yuan, R.; Chai, Y. Q. *ACS Appl. Mater. Interfaces* **2016**, *8* (20), 12968−12975.
(26) Jiang, D.; Du, X. J.; Liu, Q.; Zhou, L.; Qian, J.; Wang, K. *ACS Appl. Mater. Interfaces* **2015**, *7* (5), 3093−3100.
(27) Yu, B.; Wei, H.; He, Q. J.; Ferreira, C. A.; Kutyreff, C. J.; Ni, D.; Rosenkrans, Z. T.; Cheng, L.; Yu, F. Q.; Engle, J. W.; Lan, X. L.; Cai, W. *Angew. Chem., Int. Ed.* **2018**, *57* (1), 218−222.
(28) Pedroso, C. C.; Carvalho, J. M.; Rodrigues, L. C.; Hölsä, J.; Brito, H. F. *ACS Appl. Mater. Interfaces* **2016**, *8* (30), 19593−19604.
(29) Walcarius, A. *Chem. Soc. Rev.* **2013**, *42* (9), 4098−4140.
(30) Wang, Z. Y.; Zhao, J.; Bao, J. C.; Dai, Z. H. *ACS Appl. Mater. Interfaces* **2016**, *8* (1), 827−833.
(31) Grossmann, T. N.; Röglin, L.; Seitz, O. *Angew. Chem., Int. Ed.* **2007**, *46* (27), 5223−5225.
(32) Miller, B. R.; Wei, T. Q.; Fields, C. J.; Sheng, P.; Xie, M. Y. *RNA* **2018**, *24* (12), 1871−1877.
(33) Mohsen, M. G.; Kool, E. T. *Acc. Chem. Res.* **2016**, *49* (11), 2540−2550.
(34) Hu, Y. W.; Cecconello, A.; Idili, A.; Ricci, F.; Willner, I. *Angew. Chem., Int. Ed.* **2017**, *56* (48), 15210−15233.
(35) Guo, B. Y.; Sheng, Y. Y.; Zhou, K.; Liu, Q. S.; Liu, L.; Wu, H. C. *Angew. Chem., Int. Ed.* **2018**, *57* (14), 3602−3606.
(36) Yang, H.; Hou, Q. F.; Wang, S. J.; Guo, D. H.; Hu, G. X.; Xu, Y.; Tai, J.; Wu, X.; Yu, D. F.; Wang, J. B. *Chem. Commun.* **2018**, *54* (76), 10679−10682.
(37) Yang, H.; Zhuang, Y. M.; Hu, H.; Du, X. X.; Zhang, C. X.; Shi, X. Y.; Wu, H. X.; Yang, S. P. *Adv. Funct. Mater.* **2010**, *20* (11), 1733−1741.
(38) Li, R. Y.; Tu, W. W.; Wang, H. S.; Dai, Z. H. *Anal. Chem.* **2018**, *90* (15), 9403−9409.
(39) Tang, R.; Xue, J. P.; Xu, B. G.; Shen, D. W.; Sudlow, G. P.; Achilefu, S. *ACS Nano* **2015**, *9* (1), 220−230.
(40) Liu, J. L.; Tang, Z. L.; Zhang, J. Q.; Chai, Y. Q.; Zhuo, Y.; Yuan, R. *Anal. Chem.* **2018**, *90* (8), 5298−5305.
(41) Zhao, Y. M.; Zhai, Q. F.; Dong, D. S.; An, T.; Gong, S.; Shi, Q. Q.; Cheng, W. L. *Anal. Chem.* **2019**, *91* (10), 6569−6576.
(42) Xu, Z. Q.; Liao, L. L.; Chai, Y. Q.; Wang, H. J.; Yuan, R. *Anal. Chem.* **2017**, *89* (16), 8282−8287.

DOI: 10.1021/acs.analchem.9b03071
Anal. Chem. 2019, 91, 12038−12045